Journal of Thermal Biology 83 (2019) 60–68

Contents lists available at ScienceDirect

Journal of Thermal Biology

journal homepage: www.elsevier.com/locate/jtherbio

Air-conditioning characteristics in nasal cavity models exhibiting nasal cycle states

Seongsu Byun[a], Seung-Kyu Chung[b], Yang Na[a,*]

[a] Department of Mechanical Engineering, Konkuk University, Seoul, Republic of Korea
[b] Department of Otorhinolaryngology: Head and Neck Surgery, Samsung Medical Center, Sungkyunkwan University, School of Medicine, Seoul, Republic of Korea

ARTICLE INFO

Keywords:
Nasal cycle
Temperature
Relative humidity
Computational fluid dynamics
Water vapor transfer

ABSTRACT

The air-conditioning characteristics in nasal cavity models obtained from two subjects exhibiting different degrees of the nasal cycle states in terms of the airflow partition were investigated using computational fluid dynamics. A constant inspiratory flow rate of approximately 250 mL/s was considered, and the air temperature and relative humidity at the inlet were assumed to be 25 °C and 35%, respectively. The air-conditioning capacities of the congested and decongested sides were assessed by the amounts of epithelial heat and water vapor transferred to the inhaled air through the airway from the nostrils to the end of the septum. The results revealed that the air temperature and relative humidity near the end of the septum, respectively, reached approximately 31.4–32.5 °C and 81.4–88.0% in the decongested sides and 34.0–35.9 °C and 95.3–100% in the congested sides. The differences seen in the air temperatures and relative humidity between the congested and decongested sides were found to be larger in the cavity model that showed a larger degree of reciprocal change in the airflow rate. From a fluid mechanics perspective, while the congested side is in a rest period during the nasal cycle such that a lower amount of airflow is transported through it, this side, in effect, works to provide assistive air-conditioning capacity to the nasal cavity and aids when insufficiently conditioned airflow passes through the decongested side so that the inhaled air merging after the septum can approach the alveolar condition favorably through the nasopharynx.

1. Introduction

The nasal cycle refers to the spontaneous changes in the nasal cavity due to alternating congestion and decongestion of the nasal airways resulting in a fluctuation in the airflow rate between the left and right nasal passages. This phenomenon, however, may be observed as having a wide range of patterns due to the differences in the airflow partition, unilateral nasal patency, and duration time of the cycle observed among subjects. For example, up to 80% of subjects exhibit periodic and reciprocal changes in unilateral nasal resistance (Heetderks, 1927; Stoksted, 1953; Hasegawa and Kern, 1978) while others exhibit irregular patterns (Hasegawa and Kern, 1978; Gilbert and Rosenwasser, 1987; Flanagan and Eccles, 1997; Moore and Eccles, 2012). The frequency of the nasal cycle has also been reported to show significant individual variations, but typical reciprocal changes in nasal airflow are known to occur on a time-scale in the range of 0.5–3.0 h (Flanagan and Eccles, 1997).

There have been discussions on the role of the nasal cycle in nasal physiology (Hasegawa and Kern, 1978; Eccles, 2000). The periodic fluctuation of airflow partitioning has been typically correlated with the burden-sharing aspects of the left and right sides of the nasal cavity (Eccles, 2000; Lang et al., 2003; Moore and Eccles, 2012). In fact, Jo et al. (2015) showed that the flow partition ratio could be skewed to as much as 1:4 between the congested and decongested sides. Also, the unilateral nasal resistance of the decongested side could be reduced to about 12–13% of that of the congested side. Therefore, the physiological role of the nasal cycle can be interpreted in terms of its role in providing a rest period to the nasal cavity from the flow dynamics viewpoint.

Several studies have suggested that the air-conditioning capacity of the nasal cavity is important in maintaining physiological homeostasis (Rouadi et al., 1999; Lindemann et al., 2002; Wolf et al., 2004; Elad et al., 2008; Kim et al., 2017). During a quiet breathing situation, the inhaled air is conditioned so that it reaches approximately 31–34 °C and over 90% relative humidity (RH) before it reaches the pharynx (Rouadi et al., 1999; Keck et al., 2000; Naftali et al., 2005; Kim et al., 2017). Achieving a near alveolar condition before reaching the lungs is important to protect the alveolar lining. However, it is uncertain whether

* Corresponding author. Department of Mechanical Engineering, Konkuk University, Seoul, 05029, Republic of Korea.
E-mail address: yangna@konkuk.ac.kr (Y. Na).

https://doi.org/10.1016/j.jtherbio.2019.05.004
Received 18 January 2019; Received in revised form 6 April 2019; Accepted 10 May 2019
Available online 13 May 2019

the air inhaled through the decongested side can be sufficiently conditioned during the nasal cycle states. A proper assessment of the division of the air warming and humidification tasks between the congested and decongested airway passages is likely to be important, but there is only limited information regarding this in the existing literature. Patel et al. (2015) investigated the importance of the nasal cycle before and after surgery in patients experiencing nasal airway obstruction. They observed sizable fluctuations both in nasal resistance and mucosal cooling between the nasal passages during the nasal cycle. Although only overall information on the average heat flux was discussed in their work, their results suggest that the level of the air-conditioning duty also alternates between sides in phases during the nasal cycle states.

The objective of the present work is to investigate the physiological role of the nasal cycle in the air-conditioning capacities of the congested and decongested sides of the nasal cavity. Nasal cavity models were constructed using the CT data of two subjects exhibiting different degrees of the nasal cycle states. The air-conditioning characteristics were examined by the temperature and water vapor concentration fields as well as the velocity fields.

2. Material and methods

2.1. Construction of the nasal cavity models

CT images of a cohort of 32 patients were visually reviewed, and two patients (a 29-year-old male and a 34-year old female) exhibiting obvious alternating changes in turbinate thickness between the nasal passages due to the nasal cycle were chosen similar to the study of Jo et al. (2015). The male patient (patient 1) was found to have obvious reciprocal changes, whereas the female patient (patient 2) had rather mild reciprocal variations. Both patients suffered from chronic rhinosinusitis but did not have a history of surgical intervention for the medical management of the nasal obstruction.

Computational models were created using the CT data of the two patients after the existence of the nasal cycle was confirmed. CT images were taken during a routine clinical procedure and were processed using the computer-aided design software Vworks v4.0 (Cybermed Inc., Seoul, Korea). This study was approved by the Institutional Review Board of the Samsung Medical Center, Seoul, Korea. The numerical models used in the study by Jo et al. (2015) were improved by adding a large portion of the faces to the nasal cavities as shown in Fig. 1. These reconstructed computational models are expected to demonstrate a more realistic inflow through the nostrils than in those used in the Jo et al. study (2015) and, thus, would result in a more accurate assessment of the velocity field inside the nasal airway and the flow rate partition ratios between the left and right airways. The geometric characteristics of these models for the patients are exhibited in Fig. 2. To be consistent with the notations of Jo et al. (2015), Case 1 and Case 2 represent the nasal cavity models of patient 1 and patient 2, respectively. In addition, Case 1-L refers to the cavity model of patient 1 with a congested state on the left side whereas Case 1-R denotes the cavity model with a congested state on the right side. Case 2-L and Case 2-R also represent the cavity models of patient 2 with a congested state on the left and right sides, respectively.

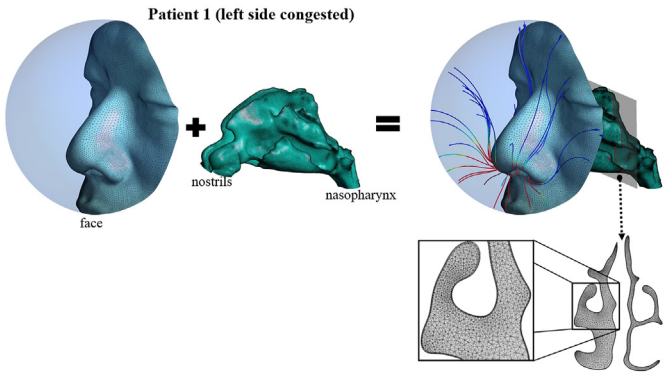

Fig. 1. Construction of computational models with approximately 8 million mesh elements.

To define the vestibule, we used an approach similar to that of Garcia et al. (2007). A 3D curve on the nasal surface was generated by intersecting a sphere with the nasal cavity. It was assumed that this curve reasonably divided the surface of nasal cavity into the vestibule and nasal cavity proper. Due to the difference in anatomical geometry of the anterior part of the nose of four cavity models, different values of the diameter of the sphere (33–35 mm, 35–38 mm, 25 mm, and 25 mm for Case1-L, Case1-R, Case2-L, and Case2-R, respectively) were used to define the vestibule.

Based on the inspiratory airflow rate of approximately 250 mL/s, the flow partition was found to vary depending on the cavity models (Table 1). Case 1 exhibited a more pronounced reciprocal change of flow rates between the nasal passages than Case 2.

2.2. Numerical details

It was assumed that the general behavior of the inhaled air during the inspiration period could be reasonably represented by a steady flow field obtained with an airflow rate of 250 mL/s. This constant airflow rate was implemented by adjusting appropriate values for the outlet pressures of each cavity model, and the resulting flow-fields were obtained using the ANSYS-Fluent R19.1 software with an assumption of a laminar flow regime.

For the evaluation of the air-conditioning capacity of the nasal cavity, both the temperature and water vapor concentration fields were also obtained by incorporating the methodology described by Kim et al. (2017). In their wall model, the respiratory epithelium is assumed to be covered with a mucus layer. The connective tissue layer—lamina propria—containing rich blood vessels underlying the epithelium is modeled as a heat reservoir maintaining a constant temperature of T_{tissue} and the mucus layer is modeled as a heat conducting layer consisting of liquid water with a thickness of δ_m. In the present work, the temperature and water vapor concentration distributions along the epithelial surface of the nasal cavity were predicted with the choices of two parameters, i.e., 5 mm for the thickness of the mucus layer (δ_m) and 36 °C for the tissue temperature (T_{tissue}), which were shown to produce the best results compared to the measurement data of Lindemann et al. (2002). Note that the interface between the mucus layer and the inhaled air is defined as the 'surface,' and the temperature at the surface, $T_{surface}$, was determined *a posteriori* after numerical convergence was achieved in the methodology by Kim et al. (2017). The RH along the surface of the nasal cavity was assumed to be 100%.

At the inlet of the computational domain, the pressure was set to zero, and the inhaled air was assumed to be at the typical atmospheric condition of 25 °C and 35% RH. At the outlet, the pressure was adjusted for each of the cavity models so that an air flow rate of approximately 250 mL/s was achieved. The vestibule area is lined with squamous epithelium, and, thus, almost no water vapor transfer to the air is allowed there. Hence, the zero-water vapor flux boundary condition at the surface was implemented using an in-house code in the form of a user-defined-function in the vestibule area. The temperature along the facial skin is known to vary depending on the location (Ariyaratnam and Rood, 1990); however, a constant value of 32 °C that was obtained in the cheek area (Ariyaratnam and Rood, 1990) was assumed for the present computation.

The computational mesh was generated using the ANSYS Meshing R19.1 software with combined tetrahedral and prism elements. As was done in previous studies with similar geometry (Jo et al., 2015; Kim et al., 2017), 7 layers of prism elements were placed along the epithelial surface to improve the numerical accuracy. The 1st prism has a

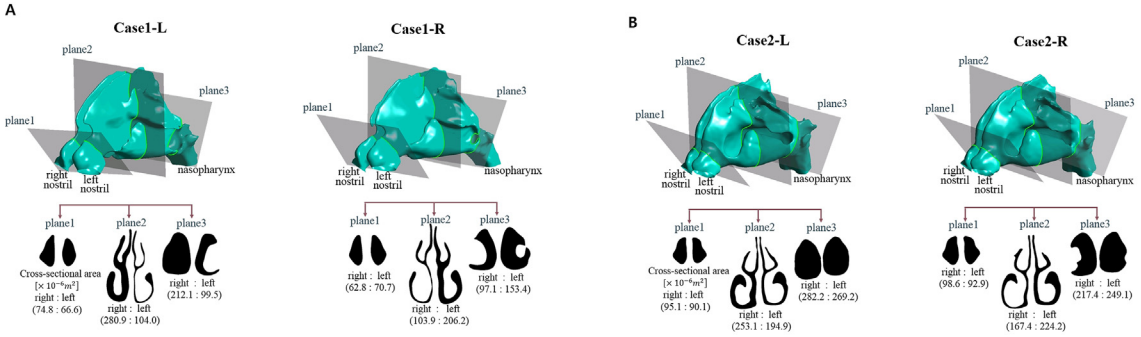

Fig. 2. Geometric characteristics of the computational models. (a) Case 1-L and Case 1-R, (b) Case 2-L, Case 2-R.

Table 1
Partition of the volume flow rate through the congested and decongested sides for the four cavity models.

Case description	Cavity model	Volume flow rate (mL/s) (right side: left side)
Case 1 (patient 1)	Case 1-L (left side congested)	203.4 : 45.1
	Case 1-R (right side congested)	60.2 : 188.3
Case 2 (patient 2)	Case 2-L (left side congested)	134.9 : 113.4
	Case 2-R (right side congested)	111.8 : 137.4

thickness of 2×10^{-5} m, and the remaining 6 prisms were generated using a growth rate of 1.1. Approximately 4 million mesh elements were found to be reasonably sufficient for the study of the velocity field by Jo et al. (2015), but an enhanced resolution with about 8 million elements was shown to be recommended for the proper evaluation of temperature and water vapor concentration fields in a similar geometry by Kim et al. (2017). Accordingly, a computational mesh was constructed using approximately 8.0 million mesh elements for the four cavity models considered in the present study.

We used mass-weighted average temperature and relative humidity to present the results of the inhaled air.

3. Results

3.1. Geometric information of nasal cavities models

The distributions of the cross-sectional areas through the airway passage from the nostrils to the nasopharynx are shown in Fig. 3. The degree of asymmetry in the cross-sectional area between the left and right sides is much larger in Case 1 than in Case 2. The geometry related quantities—airway volume and surface area of the nasal airway from the nostril to the end of the septum, surface area to volume ratio (SAVR) (Garcia et al., 2007), flow partition ratio, and unilateral nasal resistance—are summarized in Table 2. Although the airway volume of the decongested side is much larger than that of the congested side for both Case 1 and Case 2, the difference in surface areas was found to be small. As a result, the SAVR is considerably larger in the congested sides. Consistent with the reduced volume flow rate through the congested sides, the unilateral nasal resistance defined between the nostrils and choanae is also much larger on these sides.

3.2. Temperature and water vapor concentration fields

The temperature distributions along the epithelial surface are shown in Fig. 4. In Case 1-L, the surface temperature was found to be higher in the posterior part of the nasal cavity on the congested side (Fig. 4a). Note that the geometric characteristics for Case 1-L are that the cross-sectional areas of the congested and decongested sides are almost identical from the nostril to the anterior portion of the middle meatus; however, the cross-sectional area of the decongested side is much larger than that of the congested side thereafter. Similar behavior of surface temperature distribution was seen in Case 1-R but to a lesser degree than in Case 1-L (Fig. 4b). Notably, the difference in the cross-sectional area between the congested and decongested sides posterior of the middle meatus is smaller in Case 1-R than in Case 1-L. In Case 2, where the reciprocal change of volume flow rate is not as obvious as in Case 1 (Table 1), the difference in the surface temperature distribution is also not obvious as seen in Case 1 (Fig. 4c–d).

The distributions of surface heat flux are similar to those of surface temperatures (Fig. 5). Consequently, the heat supply from the epithelial surface to the inhaled air can occur throughout the main airway passage on the decongested sides, but it is limited to the anterior region of

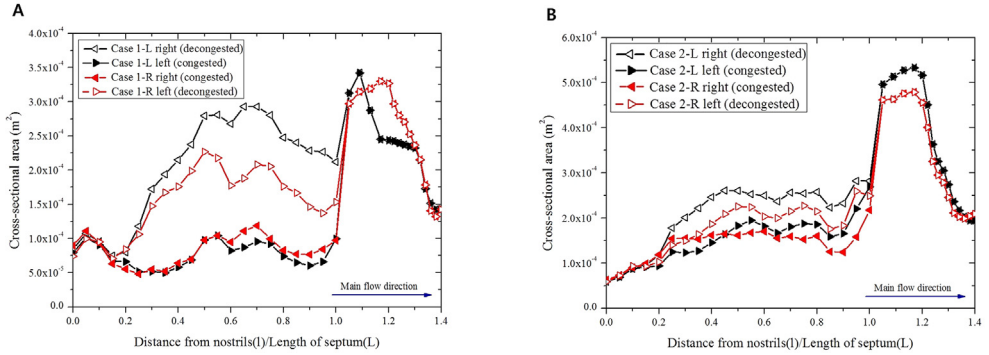

Fig. 3. Distribution of the cross-sectional area for the planes perpendicular to the local flow direction. (a) Case 1, (b) Case 2.

Table 2
Geometric characteristics of the four cavity models.

	Case 1 (patient 1)				Case 2 (patient 2)			
	Case 1-L (left side congested)		Case 1-R (right side congested)		Case 2-L (left side congested)		Case 2-R (right side congested)	
	right	left	right	left	right	left	right	left
airway volume from nostril to choanae [10^3 mm^3]	15.25	6.04	6.55	11.75	13.70	10.36	9.68	11.88
surface area from nostril to choanae [10^3 mm^2]	8.58	8.21	8.22	8.20	8.64	8.91	8.72	8.47
SAVR (surface area to volume ratio) [mm^{-1}]	0.563	1.360	1.254	0.698	0.631	0.860	0.901	0.713
flow partition ratio [%]	81.8	18.2	24.2	75.8	54.3	45.7	44.9	55.1
unilateral nasal resistance [Pa·s/(m·mL)]	0.0254	0.243	0.188	0.0256	0.0132	0.0249	0.0325	0.0101

the middle meatus on the congested sides for Case 1 (Fig. 5a–b). This implies that the posterior part of the cavity on the congested sides lose less heat to the air and, thus, maintain a higher surface temperature. Again, the difference in surface heat flux between the congested and decongested sides is hardly seen in Case 2 (Fig. 5c–d).

The water vapor flux from the surface is shown in Fig. 6. The existence of a high correlation between the water vapor and surface heat flux is evident. Specifically, the water vapor transfer from the surface to the air is restricted to the nasal valve area and the anterior of the middle turbinate on the congested sides and it is more distributed along the main airway passage on the decongested sides for Case 1 (Fig. 6a). Note that the water vapor flux does not exist in the vestibule area due to a zero-flux boundary condition set there. As with the behavior shown in Fig. 5c–d, the region having non-negligible water vapor transfer at the surface is distributed in larger areas on both the congested and decongested sides in Case 2 where the reciprocal change is not as obvious as in Case 1 (Fig. 6c–d).

The temperature variation of the inhaled air is displayed in Fig. 7. The temperature of the air approaching the end of the septum was found to be higher on the congested sides of both Case 1 and Case 2. Since the air temperature change is determined by the balance between the volume flow rate of the air and the amount of heat transfer from the epithelial surface to the air, several parameters relevant to air-conditioning characteristics were examined and summarized in Table 3. Although the amount of total heat transfer from the surface to the air is less on the congested sides, the much lower volume flow rate (as shown in Table 2) resulted in a higher temperature rise of the air by the end of the septum on this side for Case 1. For example, the air temperature in the decongested and congested sides, reached about 31.6 and 35.9 °C for Case 1-L and 31.4 and 35.7 °C for Case 1-R, respectively (Fig. 7a). A similar behavior is seen for the relative humidity distribution in Fig. 8. In brief, the total amount of water vapor transported from the surface to the air is lower on the congested sides for Case 1; however, the relative humidity of the air reached approximately 100% by the end of the septum on these sides for Case 1-L and Case 1-R, while the relative humidity was approximately 81.4–82.3% for Case 1-L and Case 1-R in the decongested sides (Fig. 8a).

When the nasal cycle is less obvious in Case 2, the general behaviors

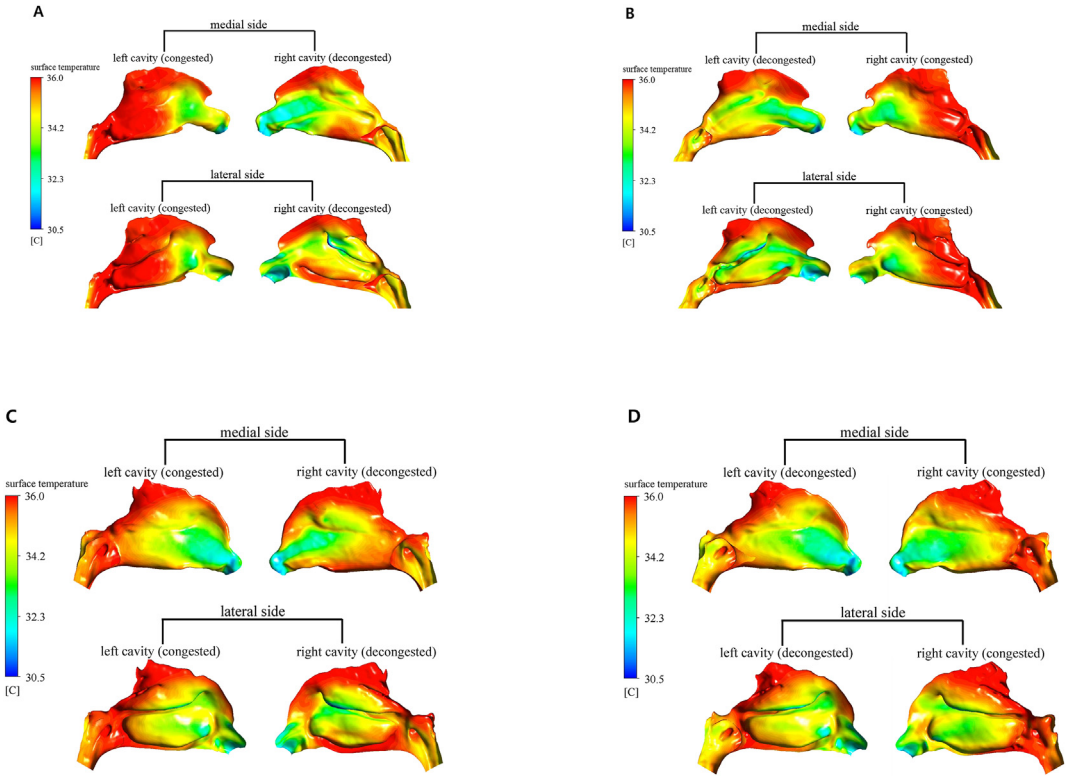

Fig. 4. Distribution of surface temperature. (a) Case 1-L, (b) Case 1-R, (c) Case 2-L, (d) Case 2-R.

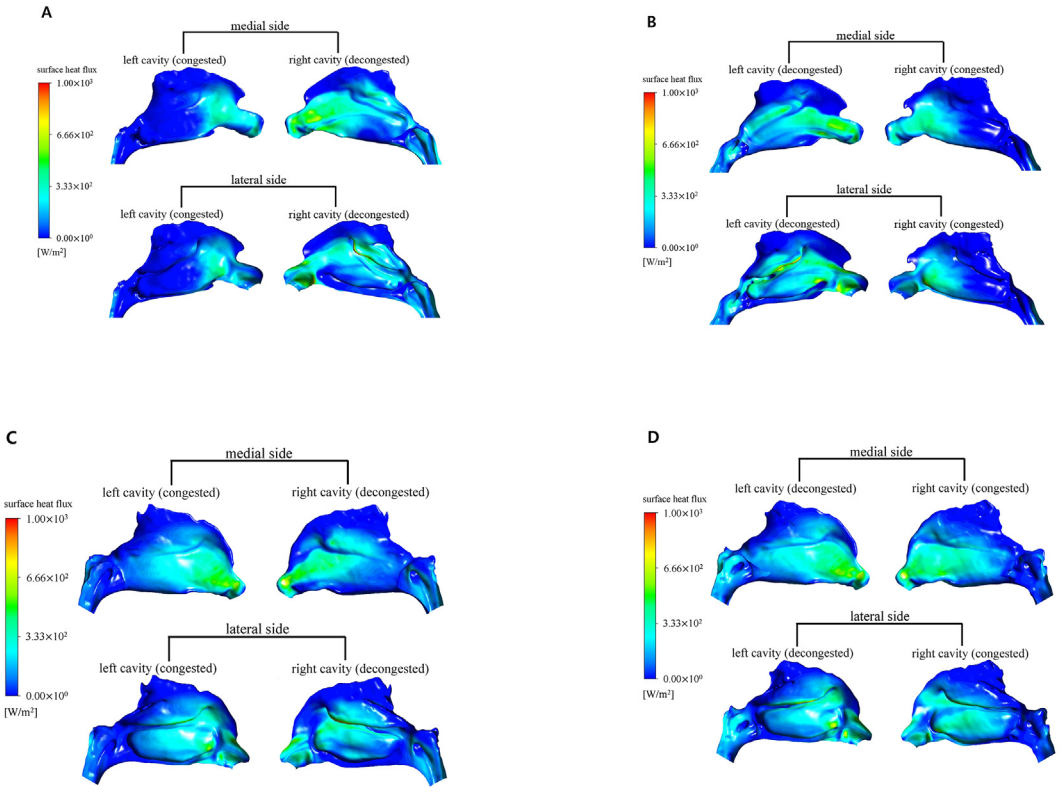

Fig. 5. Distribution of surface heat flux. (a) Case 1-L, (b) Case 1-R, (c) Case 2-L, (d) Case 2-R.

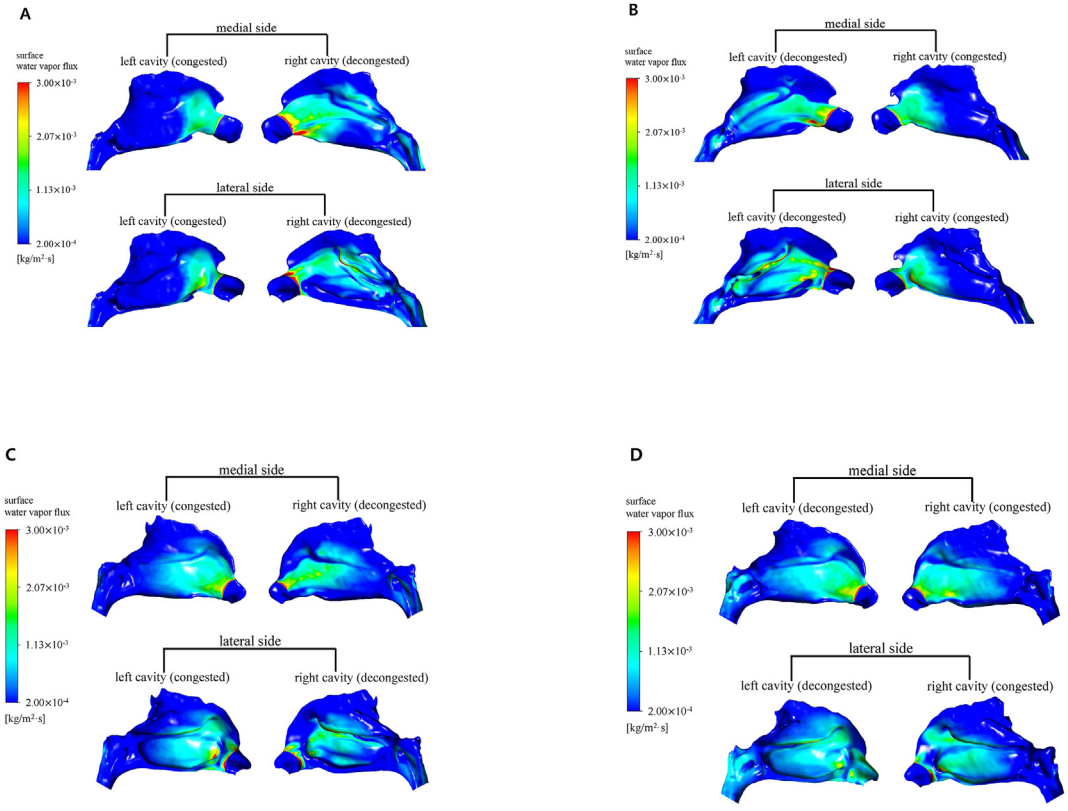

Fig. 6. Distribution of surface water vapor flux. (a) Case 1-L, (b) Case 1-R, (c) Case 2-L, (d) Case 2-R.

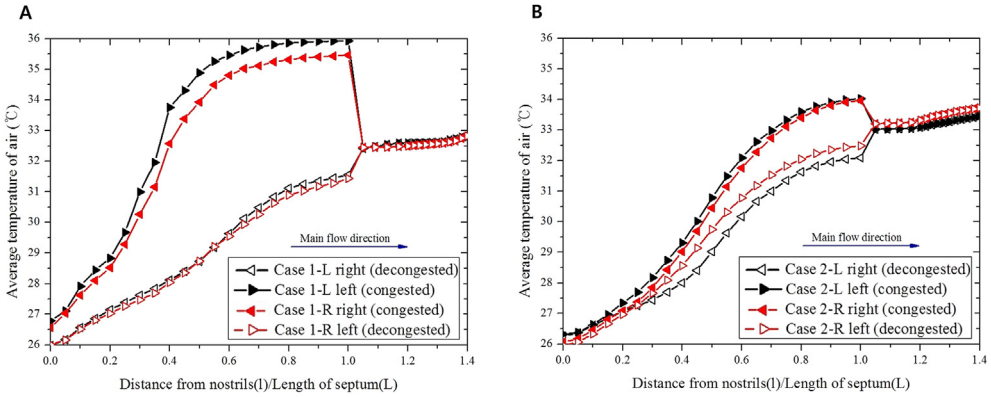

Fig. 7. Distribution of average temperature of inhaled air along the distance from nostrils.

Table 3
Air-conditioning characteristics of the four cavity models.

	Case 1 (patient 1)				Case 2 (patient 2)			
	Case 1-L (left side congested)		Case 1-R (right side congested)		Case 2-L (left side congested)		Case 2-R (right side congested)	
	right	left	right	left	right	left	right	left
heat flux at surface [W/m^2]	156.2	61.1	80.2	147.6	108.8	117.3	121.7	126.4
total heat transfer rate at surface [W]	1.340	0.502	0.659	1.210	0.940	1.045	1.062	1.070
air temperature near the end of septum [°C]	31.6	35.9	35.7	31.4	32.1	34.0	34.0	32.5
surface water vapor flux [10^{-4} kg/(s·m^2)]	4.72	1.96	2.55	4.52	3.36	3.77	3.79	3.90
total water vapor transfer rate at surface [10^{-6} kg/s]	4.05	1.61	2.10	3.71	2.90	3.36	3.31	3.31
air humidity near the end of septum [%]	82.3	100.0	99.7	81.4	83.0	95.3	95.5	88.0

of the air temperature and relative humidity distributions are similar to those displayed by Case 1; thus, the air temperatures and relative humidity are higher on the congested sides (Figs. 7–8). However, the differences in the air temperature and relative humidity between the congested and decongested sides were found to be reduced (Figs. 7b–8b). Air temperature differences were reduced to 1.9 °C for Case 2-L and 1.5 °C for Case 2-R, and the differences in relative humidity between the two sides were also reduced to 12.3% for Case 2-L and 7.5% for Case 2-R.

Correlations between the air-conditioning function and the nasal geometry were investigated using the information listed in Tables 1–3 Fig. 9a–b shows that both the heat and water vapor fluxes at the surface decrease with SAVR for Case 1 where the flow partition is highly skewed. However, in Case 2 where the reciprocal change is not as large as in Case 1, the behavior seen in Case 1 is not clearly observed. Fig. 9c shows that epithelial heat flux also decreases with nasal resistance for Case 1. This behavior is consistent with the observation seen in Fig. 9a–b noting that the congested sides have a larger nasal resistance and SAVR than the congested sides. Fig. 9d suggests that the epithelial heat flux increases with the flow partition ratio for Case 1. That is, the decongested sides provide larger heat fluxes from the epithelial surface than the congested sides for this cavity model.

4. Discussion

The air-conditioning characteristics during the nasal cycle were investigated numerically with four nasal cavity models that represent both the congested and decongested states of the nasal cycle. An inspiratory air flow rate of approximately 250 mL/s was considered. In addition to the velocity field, the temperature and water vapor concentration fields were calculated to assess the distributions of air temperature and relative humidity using the methodology described by Kim et al. (2017).

The physiological role of the nasal cycle is still not clearly

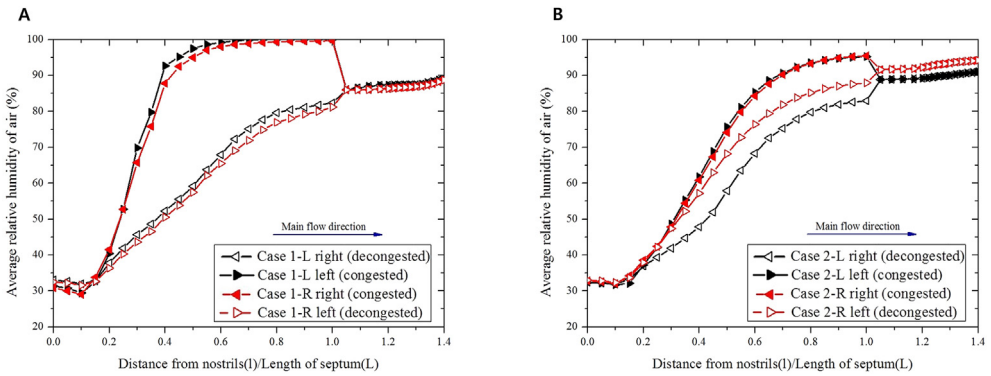

Fig. 8. Distribution of average relative humidity of inhaled air along the distance from nostrils.

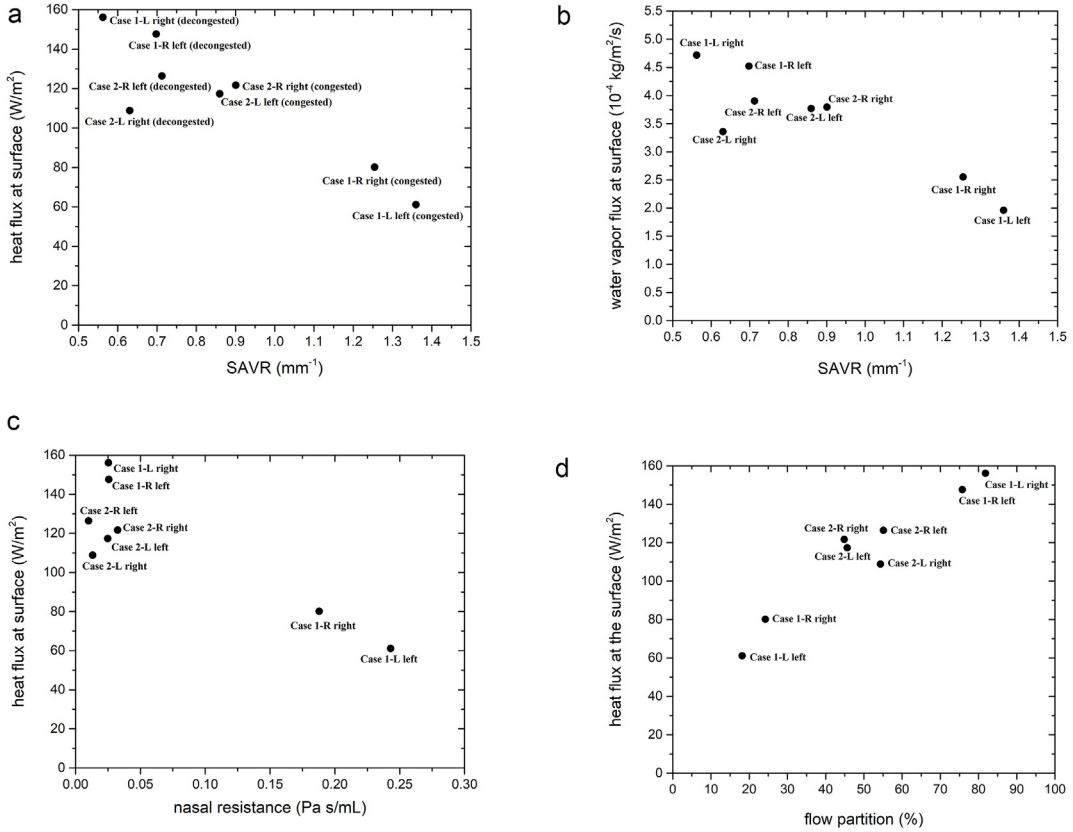

Fig. 9. Correlations between the air-conditioning function and the nasal geometry. (a) Epithelial heat flux vs. SAVR, (b) Epithelial water vapor flux vs. SAVR, (c) Epithelial heat flux vs. nasal resistance, (d) Epithelial heat flux vs. flow partition ratio.

understood, but it frequently has been linked to the alternating ease of the respiratory burden between the two nasal sides (Eccles, 2000; Lang et al., 2003; Moore and Eccles, 2012). In brief, the decongested side having the larger cross-sectional area transports a significantly increased amount of the airflow required for respiration while the congested side is in a state of rest from the standpoint of the breathing effort. For example, the volume flow rate was shown to be partitioned as approximately 82%:18% between the decongested and congested sides in Case 1-L (Table 2). In order to allow an increased airflow rate on the decongested side, the nasal resistance is reduced by enlarging the cross-sectional area resulting in a larger airway volume as shown in Tables 1 and 2

Although the overall transfer of heat and water vapor from the surface to the inhaled air was larger in the decongested side for Case 1, the larger volume or, equivalently, increased volume flow rate resulted in a lower air temperature and relative humidity on this side by the end of the septum. However, Figs. 7a–8a show that the air temperature and relative humidity right after the choanae where the two separate streams from the left and right airway passages merged approached 33 °C and 90%, respectively, for Case 1. Note that these values are in the range typically observed in the nasal cavity (Cole, 1953; Keck et al., 2000; Lindemann et al., 2002, 2003; Kim et al., 2017). Therefore, the insufficient performance of the air-conditioning duty for the heavily overloaded decongested side, due to the significantly increased airflow rate, was complemented by the assistive performance of the less loaded congested side. Without this supportive contribution of the congested side, an appropriate thermodynamic state of the air in terms of warming and humidification would not be expected to be obtained after the choanae. Noting that the epithelial heat and water vapor fluxes are not uniformly distributed over the cavity but mainly occur in the anterior portion of the middle meatus in the congested sides and through the main airway in the decongested sides (Figs. 5–6), surgical planning should be carefully designed not to cause significant disturbances in the air-condition capacity.

In a study of atrophic rhinitis (AR), Garcia et al. (2007) proposed that the main symptoms of AR, such as dryness and crusting, resulted from excessive evaporation from the mucous layer. This hypothesis can be understood by interpreting that the abnormally wide nasal cavity associated with AR, which has an average SAVR of 0.45, was not able to condition inhaled air as effectively as the decongested sides of the present cavity model for Case 1. Note that this value of SAVR is lower than the lowest value in the present investigation; however, large epithelial heat loss is expected at this low SAVR value inferred from Fig. 9a. Therefore, the epithelial surface of the nasal cavities for AR subjects who have a low SAVR maintained permanently is likely to experience an excessively evaporated environment constantly. This physical interpretation is also consistent with the observation made by Drettner et al. (1977) that atrophic noses do not condition the air as effectively as normal ones.

Although the inhaled air flow was shown to be sufficiently conditioned after the choanae even in Case 1-L where the flow partition is skewed, there may be an upper limit of the flow partition ratio—or the maximum airway volume of the decongested side—beyond which the air temperature and humidity regulation to the near alveolar condition is not possible. Therefore, it would be interesting to find an upper limit of the flow partition ratio from the viewpoint of air-conditioning capacity. When the volume increase of the decongested side experiencing nasal cycle states is combined with the effect of symptoms, such as septal deviation or AR, the increased amount of air through the decongested side may result in an insufficiently conditioned state after the choanae that may cause a burden to the airway leading to the lungs.

Several limitations of the present study need to be mentioned. The present results suggest that the congested side is not completely dormant but is still active to provide the air-conditioning capacity to

compensate for the deficiency in the decongested side. Since only four cavity models have been examined, this speculation requires more evidence from further studies. The nasal cycle appears in various forms regarding the duration time, the difference in the cross-sectional area of the cavity, and the flow partition ratio; therefore, future studies are required to define the physiological outcome of the nasal cycle from the standpoint of air-conditioning capacity.

Additionally, an issue arises due to assuming a constant flow rate of 250 mL/s that represents an average flow rate during an inspiration period. For a quiet breathing situation at a typical frequency of 15 breaths/min, Doorly et al. (2008) showed that a quasi-steady approximation is valid for a Womersley number of less than 3. Kim et al. (2017) showed that the Womersley number is in the range of 0.5–1.75 in the region anterior to the choanae where significant epithelial heat and water vapor transfer occur at the given flow rate of 250 mL/s. Thus, it was assumed that the present quasi-steady approximation is reasonably acceptable except in the region posterior to the choanae. Nevertheless, a transient simulation is required in future studies to elucidate the inertial effect on the air-conditioning capacity in the nasal cycle.

5. Conclusion

The air-conditioning capacity was examined using computational fluid dynamics for the nasal cavity models exhibiting alternating nasal cycle states. A constant inspiratory flow rate of approximately 250 mL/s was considered. In addition to the velocity field, both the temperature and water vapor concentration fields were obtained to assess the temperature and humidity distributions of the inhaled air through the nasal cavity. Even if the total amounts of heat and water vapor transferred from the epithelial surface to the air are larger through the decongested side, it is possible that the air-conditioning capacity is not sufficient enough to properly process the significantly increased amount of airflow passing through this side. For example, the temperature and relative humidity of the air were found to be approximately 31.6 °C and 82.3% on the decongested side while higher values of about 35.9 °C and 100% were obtained on the congested side for the cavity model exhibiting a flow partition ratio of approximately 82%:18%. However, for the cavity models showing less obvious nasal cycle states, the differences in the air temperature and relative humidity between the congested and decongested sides were found to be reduced. Therefore, the air-conditioning requirement for the congested side is thought to be regulated by the amount of the airflow partition ratio; thus, it is physiologically important for the inhaled air to reach the alveolar condition after the choanae.

Conflicts of interest

The authors declare that they have no conflicts of interest.

Acknowledgments

This work was supported by the National Research Foundation (NRF) of Korea grant funded by the Korean government (MSIP) (No. NRF-2016R1A2B1007248).

References

Ariyaratnam, S., Rood, J.P., 1990. Measurement of facial skin temperature. J. Dent. 18 (5), 250–253. https://doi.org/10.1016/0300-5712(90)90022-7.

Cole, P., 1953. Further observations on the conditioning of respiratory air. J. Laryngol. Otol. 67, 669–681. https://doi.org/10.1017/S0022215100049161.

Doorly, D.J., Taylor, D.J., Schroter, R.C., 2008. Mechanics of airflow in the human nasal airways. Respir. Physiol. Neurobiol. 163, 100–110. https://doi.org/10.1016/j.resp.2008.07.027.

Drettner, B., Falck, B., Simon, H., 1977. Measurements of the air conditioning capacity of the nose during normal and pathological conditions and pharmacological influence. Acta Oto-Laryngol. Stockh. 84, 266–277. https://doi.org/10.3109/00016487709123966.

Eccles, R., 2000. Nasal airflow in health and disease. Acta Otolaryngol. 120, 580–595. https://doi.org/10.1080/000164800750000388.

Elad, D., Wolf, M., Keck, T., 2008. Air-conditioning in the human nasal cavity. Respir. Physiol. Neurobiol. 163, 121–127. https://doi.org/10.1016/j.resp.2008.05.002.

Flanagan, P., Eccles, R., 1997. Spontaneous changes of unilateral nasal airflow in man. A re-examination of the 'nasal cycle'. Acta Oto-Laryngol. Stockh. 117, 590–595. https://doi.org/10.3109/00016489709113443.

Garcia, G.J.M., Bailie, N., Martins, D.A., Kimbell, J.S., 2007. Atrophic rhinitis: A CFD study of air conditioning in the nasal cavity. J. Appl. Physiol. 103, 1082–1092. https://doi.org/10.1152/japplphysiol.01118.2006.

Gilbert, A.N., Rosenwasser, A.M., 1987. Biological rhythmicity of nasal airway patency: A re-examination of the 'nasal cycle'. Acta Oto-Laryngol. Stockh. 104, 180–186. https://doi.org/10.3109/00016488709109065.

Hasegawa, M., Kern, E.B., 1978. Variations in nasal resistance in man: A rhinomanometric study of the nasal cycle in 50 human subjects. Rhinology 16, 19–29. https://doi.org/10.1177/000348948209100125.

Heetderks, D.R., 1927. Observations on the reaction of normal nasal mucous membrane. Am. J. Med. Sci. 174, 231–244.

Jo, G., Chung, S.-K., Na, Y., 2015. Numerical study of the effect of the nasal cycle on unilateral nasal resistance. Respir. Physiol. Neurobiol. 219, 58–68. https://doi.org/10.1016/j.resp.2015/08.006.

Keck, T., Leiacker, R., Heinrich, A., Kühnemann, S., Rettinger, G., 2000. Humidity and temperature profile in the nasal cavity. Rhinology 38, 167–171.

Kim, D.-W., Chung, S.-K., Na, Y., 2017. Numerical study on the air conditioning characteristics of the human nasal cavity. Comput. Biol. Med. 86, 18–30. https://doi.org/10.1016/j.compbiomed.2017.04.018.

Lang, C., Grützenmacher, S., Mlynski, B., Plontke, S., Mlynski, G., 2003. Investigating the nasal cycle using endoscopy, rhinoresistometry, and acoustic rhinometry. The Laryngoscope 113, 284–289. https://doi.org/10.1097/00005537-200302000-00016.

Lindemann, J., Leiacker, R., Rettinger, G., Keck, T., 2002. Nasal mucosal temperature during respiration. Clin. Otolaryngol. 27, 135–139. https://doi.org/10.1046/j.1365-2273.2002.00544.x.

Lindemann, J., Leiacker, R., Rettinger, G., Keck, T., 2003. The relationship between water vapour saturation of inhaled air and nasal patency. Eur. Respir. J. 21, 313–316. https://doi.org/10.1183/09031936.03.00061103.

Moore, M., Eccles, R., 2012. Normal nasal patency: Problems in obtaining standard reference values for the surgeon. J. Laryngol. Otol. 126, 563–569. https://doi.org/10.1017/S002221511200045X.

Naftali, S., Rosenfeld, M., Wolf, M., Elad, D., 2005. The air-conditioning capacity of the human nose. Ann. Biomed. Eng. 33, 545–553. https://doi.org/10.1007/s10439-005-2513-4.

Patel, R.G., Garcia, G.J.M., Frank-Ito, D.O., Kimbell, J.S., Rhee, J.S., 2015. Simulating the nasal cycle with computational fluid dynamics. Otolaryngol. Head Neck Surg. 152 (2), 353–360. https://doi.org/10.1177/0194599814559385.

Rouadi, P., Baroody, F.M., Abbott, D., Naureckas, E., Solway, J., Naclerio, R.M., 1999. A technique to measure the ability of the human nose to warm and humidify air. J. Appl. Physiol. 87, 400–406. https://doi.org/10.1152/jappl.1999.87.1.400.

Stoksted, P., 1953. Rhinometric measurements for determination of the nasal cycle. Acta Otolaryngol. (Suppl. 109), 159–175. https://doi.org/10.3109/00016485309132516.

Wolf, M., Naftali, S., Schroter, R.C., Elad, D., 2004. Air-conditioning characteristics of the human nose. J. Laryngol. Otol. 118, 87–92. https://doi.org/10.1258/002221504772784504.

Seongsu Byun received his BS degree in mechanical engineering from Konkuk University, Korea. Currently, he is a graduate student in the Department of Mechanical Engineering at Konkuk University. He is actively involved in a research project in the area of computational fluid dynamics applications in biomechanics. His specialty lies in the segmentation of human CT images, computer-aided design, and computational fluid dynamics. He has been conducting a series of simulations for the present study.

Seung-Kyu Chung graduated from the College of Medicine, Yonsei University, Korea, and received his masters and PhD degrees in medicine from Yonsei University. Currently, he is working as a professor in the Department of Otorhinolaryngology-Head and Neck Surgery in the Samsung Medical Center and in the School of Medicine at Sungkyunkwan University, Korea. His research interests are 3D anatomy and physiology of the human nasal cavity especially via computational fluid dynamics. He is involved in the construction of computational models of nasal cavities and in the physiological interpretation of the present computational results.

Yang Na received his B.S. and M.S. degrees in mechanical engineering from Seoul National University, Korea, and a PhD degree from Stanford University, U.S.A. He is currently working as a professor in the Department of Mechanical Engineering, Konkuk University, Korea. His research interest lies in the area of computational fluid dynamics, heat transfer, and human nasal physiology. He has been working to develop a numerical methodology for the prediction of heat and water vapor transfer in the nasal cavity for the purpose of studying nasal physiology by examining air temperature and relative humidity distributions inside the nasal cavity.